Effect of Unbalance on Positive Sequence Synchrophasor, Frequency and ROCOF Estimations

Paolo Castello, *Member*, *IEEE*, Roberto Ferrero, *Member*, *IEEE*,
Paolo Attilio Pegoraro, *Member*, *IEEE*, Sergio Toscani, *Member*, *IEEE*

***Abstract*— Phasor Measurement Units (PMUs) are the measurement devices fostering the transformation of electric power networks towards the Smart Grid paradigm. They should accurately measure synchrophasors, frequency and rate of change of frequency (ROCOF), so that the management and control applications relying on PMU-based distributed monitoring system can operate effectively. Commercial PMUs performance is typically guaranteed by the compliance with the IEEE standard C37.118.1, which is focused on PMUs for power transmission systems and defines testing conditions and error limits. However, actual operating conditions are much more variable than those covered by the standard, especially when PMUs are used in distribution networks. In particular, the standard does not consider unbalance, which may be negligible neither in transmission nor in distribution grids. For the first time, this paper analyzes the impact of unbalance on the accuracy of four of the most significant classes of signal processing algorithms for PMU measurements. Synchrophasor, frequency and ROCOF estimation performance under different unbalance conditions is investigated in the test cases suggested by the IEEE C37.242-2013 guide. Novel analytic expressions to predict the errors are derived and validated, and they are proved to be useful for an effective implementation of PMU algorithms intended for both distribution and transmission systems.**

***Index Terms*— Frequency estimation, Phase measurement, Phasor Measurement Units, Rate of Change Of Frequency (ROCOF), Unbalanced Three-phase Electric Systems, Voltage Measurement**

I. Introduction

PHASOR Measurement Units (PMUs) are expected to become the main tool for electrical power networks monitoring. PMUs are synchronized with respect to coordinated universal time (UTC), thus allowing voltage and current amplitudes and phase angles, frequency and Rate Of Change Of Frequency (ROCOF) measurements to be performed in a common time reference. Large scale distributed measurement systems can be thus designed relying on PMU peculiarities. Such systems, namely wide area measurement systems (WAMS) in power transmission networks (TNs) context, can represent the future also for distribution network (DN) [1].

PMU employment in DNs is not straightforward, because of the different dynamics and characteristics typical of distribution systems [1]. DNs are made of shorter and weakly meshed lines, resulting in small phase-angle differences between nodes and will show less predictable operating conditions, due to a massive penetration of distributed and renewable energy resources. PMU algorithms that allow accurate measurements under a wide range of conditions will be one of keys to the success of PMU employment in DNs [2].

Nowadays, the starting point of PMU performance evaluation is the synchrophasor standard IEEE C37.118.1-2011 [3], along with its amendment IEEE C37.118.1a-2014 [4]. Since 2011, the standard defines the PMU measurement outputs and indicates errors limits under specific test cases. The test signals and requirements are used to define two classes (P and M) of compliance. Prescriptions are given in terms of reporting rate, accuracy, step response, and latency, and examples of PMU algorithms for P and M classes are reported in [3], Annex C.

In the literature, particular attention has been devoted to the identification of techniques that are well-suited to PMU implementation and to the design of algorithms that allow complying with the requirements of the standard. The test conditions indicated in [3] are often a common ground to compare the proposed methods. Many algorithms have been defined (an overview can be found in [5]) and characterized by means of both simulations [6], [7] and experimental tests [8], [9]. Nevertheless, it has become clear that PMU algorithms, particularly in DN framework, require a deeper testing to cover more realistic cases. For instance, some aspects of narrow- and wide-band noise impact are assessed in [10], [11]. The guide IEEE C37.242-2013 [12] that has been published to help the calibration, installation and testing of PMUs, reflects these emerging discussions. The guide provides a detailed description of the procedures and of the conditions to perform PMU testing from a practical perspective. It also suggests performing additional tests, with respect to those imposed by [3], considering unbalanced three-phase inputs.

In practical power systems the positive sequence synchrophasor carries most information about a three-phase quantity. For this reason, accurate positive sequence synchrophasor estimation is vital for state estimation as well as for grid control and automation. It is worth noticing that these applications are mostly based on a positive sequence representation of the system.

But most important, [3] defines a unique system frequency for each set of three-phase quantities that is the angular speed of the positive sequence synchrophasor in a GPS-synchronized reference frame. In fact, reference P-class and M-class algorithms proposed by the standard (Annex C) obtain frequency and ROCOF measurements by differentiating the positive sequence synchrophasor phase angle.

For this reason, it is interesting to study how unbalance affects frequency and ROCOF measurements, other than the

positive sequence synchrophasor estimation. Voltage and current unbalance is sometimes not negligible in high-voltage systems, since it may reach levels well above 1% even during regular operation. For example, the Italian transmission system operator monitors weekly the maximum voltage unbalance for power quality assessment. The expected 95th percentile value for 2017 is 4%, but measurements show that this value was significantly exceeded in the preceding years [13]. Current unbalance is supposed to be significantly greater. Higher unbalance figures are typical of DNs (which may include unbalanced or even single-phase loads and generators) [14]. Standard EN 50160 [15] states that, under regular operation, 95% of the ten-minute voltage unbalance should be below 3%. However, this aspect is often overlooked since only few papers deal with the issues of PMU algorithms and operation under unbalance conditions for both TN and DN [16]-[19].

In [20] the impact of a negative sequence component on the estimation performed by means of the aforementioned reference algorithms and of the recently proposed space vector (SV) based algorithms [21], [22] has been discussed from both a theoretical and practical point of view. In this paper, the analysis is expanded significantly including two other techniques that are particularly studied in recent literature for application in the synchrophasor estimation context. The first one is the Taylor-Fourier filtering algorithm [23], which is specifically designed for dynamic conditions, and is representative of a large class of methods based on synchrophasor dynamic modeling. The second one is the interpolated discrete Fourier transform (IpDFT) [24] that is particularly suited to deal with short range leakage problems. In this paper, the aim is thus to cover a wide range of estimation techniques, based on different principles, under unbalance conditions and to offer a detailed analysis of the impact of this phenomenon on classes of measurement algorithms that are designed with different goals. The impact of unbalance on the estimations provided by all the algorithms can be predicted with the analytic formulas that are introduced in this paper and validated by means of simulation results under different conditions inspired by the complementary tests described in [12]. Such equations also allow having a better insight into the main contributions to the errors of synchrophasor, frequency and ROCOF measurements in three-phase unbalanced systems. On the other hand, the derived expressions may also be helpful to an effective design of PMU algorithms both for DN and TN applications.

II. Analytic Performance Prediction

Compliance tests suggested by the well-known synchrophasor measurement standard [3] are based on three-phase balanced input signals, at least for the fundamental component. Although it is not required for the certification, [12] recommends assessing PMU performance in presence of unbalance. The suggested test signals to be applied are obtained starting from a positive sequence, three-phase signal, and changing, both in phase-shift and magnitude, one of the phases. Hence, the three sinusoidal signals x_a, x_b, x_c at the frequency f_1 (corresponding to the angular frequency ω_1) can be represented by their respective phasors $\bar{X}_a$, $\bar{X}_b$, $\bar{X}_c$:

$$\begin{bmatrix} \bar{X}_a \\ \bar{X}_b \\ \bar{X}_c \end{bmatrix} = \begin{bmatrix} X_a e^{j\varphi_a} \\ X_b e^{j\varphi_b} \\ X_c e^{j\varphi_c} \end{bmatrix} = \begin{bmatrix} (1+k_x)e^{jk_a} \\ \bar{\alpha}^2 \\ \bar{\alpha} \end{bmatrix} \bar{X} \tag{1}$$

where $\bar{\alpha} = e^{j2\pi/3}$ and the coefficients k_x and k_a allow introducing magnitude and phase unbalance respectively. For the following analysis, it is convenient to describe the test signal in terms of symmetrical components. Thus, by applying the Fortescue transformation, the positive, negative and zero sequence phasors $\bar{X}_+$, $\bar{X}_-$, $\bar{X}_0$ are obtained:

$$\begin{bmatrix} \bar{X}_+ \\ \bar{X}_- \\ \bar{X}_0 \end{bmatrix} = \frac{1}{\sqrt{3}} \begin{bmatrix} 1 & \bar{\alpha} & \bar{\alpha}^2 \\ 1 & \bar{\alpha}^2 & \bar{\alpha} \\ 1 & 1 & 1 \end{bmatrix} \begin{bmatrix} \bar{X}_a \\ \bar{X}_b \\ \bar{X}_c \end{bmatrix} = \begin{bmatrix} \left[(1+k_x)e^{jk_a}+2\right] \\ \left[(1+k_x)e^{jk_a}-1\right] \\ \left[(1+k_x)e^{jk_a}-1\right] \end{bmatrix} \frac{\bar{X}}{\sqrt{3}} \tag{2}$$

It should be noticed that the negative and zero sequence phasors are exactly the same. It is worth defining the unbalance level, namely the magnitude of the ratio between negative and positive sequence phasors, that can be easily computed. Using the inverse Steinmetz transform, the time-domain test signals can be written as:

$$\begin{bmatrix} x_a(t) \\ x_b(t) \\ x_c(t) \end{bmatrix} = \frac{1}{\sqrt{2}} \left(\begin{bmatrix} \bar{X}_a \\ \bar{X}_b \\ \bar{X}_c \end{bmatrix} e^{j\omega_1 t} + \begin{bmatrix} \bar{X}_a^* \\ \bar{X}_b^* \\ \bar{X}_c^* \end{bmatrix} e^{-j\omega_1 t} \right) \tag{3}$$

where * denotes the complex conjugate operator. Using the inverse Fortescue transform:

$$\begin{bmatrix} \bar{X}_a \\ \bar{X}_b \\ \bar{X}_c \end{bmatrix} = \frac{1}{\sqrt{3}} \begin{bmatrix} \bar{X}_+ + \bar{X}_- + \bar{X}_0 \\ \bar{\alpha}^2 \bar{X}_+ + \bar{\alpha} \bar{X}_- + \bar{X}_0 \\ \bar{\alpha} \bar{X}_+ + \bar{\alpha}^2 \bar{X}_- + \bar{X}_0 \end{bmatrix} \tag{4}$$

The three-phase test signals have to be applied to the input of the PMU under test which returns the measured positive sequence synchrophasor, frequency and ROCOF. Assuming that ω_0 is the rated angular frequency of the power system, an ideal PMU should return exactly zero ROCOF, the actual frequency f_1 and a positive sequence synchrophasor $\bar{x}_+$ whose expression, as a function of time, is:

$$\bar{x}_+(t) = \bar{X}_+ e^{j(\omega_1 - \omega_0)t} \tag{5}$$

From the estimations and the actual values, the usual performance indexes, Total Vector Error (TVE), Frequency Error (FE) and ROCOF Error (RFE), must be evaluated.

It is clear that results strictly depend on the peculiar estimation technique implemented in the PMU. In this work, four types of algorithms are considered and compared. For all of them, analytic expressions that allow predicting TVEs, FEs, RFEs in case of unbalanced input have been derived.

A. Space Vector based PMUs

PMU algorithms based on the SV transformation have been firstly proposed by the authors in [21]. An improved version

[22] is characterized by higher flexibility: its performance depends on five digital filters that can be tailored to meet specific goals, for example complying with P and M classes. One of the advantages is that the results of the performance tests required by [3], [4] can be predicted by using simple analytic expressions. These formulas, as shown in the following, can be employed also to predict the accuracy in case of unbalance.

SV-based algorithms require computing the space vector $\bar{x}_{SV}$ in a reference frame rotating at the speed ω_0, corresponding to the rated frequency f_0 of the power system:

$$\bar{x}_{SV}(t) = \sqrt{\frac{2}{3}}\begin{bmatrix}1 & \bar{\alpha} & \bar{\alpha}^2\end{bmatrix}\cdot\begin{bmatrix}x_a(t)\\ x_b(t)\\ x_c(t)\end{bmatrix}e^{-j\omega_0 t} \tag{6}$$

Substituting (3) and (4) into (6) it is possible to write the expression of the SV in terms of symmetrical components:

$$\bar{x}_{SV}(t) = \left(\bar{X}_+ e^{j\omega_1 t} + \bar{X}_-^* e^{-j\omega_1 t}\right)e^{-j\omega_0 t} \tag{7}$$

As expected, the SV is unaffected by the zero-sequence term. Moreover, equations presented in [22] for the steady-state tests can be also employed to predict how unbalance affects the estimations. In fact, the negative sequence component can be seen as a harmonic disturbance characterized by a negative angular frequency $-\omega_1$. The SV approach requires designing the input filter H as well as the other filters for estimating the positive-sequence synchrophasor magnitude and phase (M and P respectively), frequency and ROCOF (F and R). Thus, introducing $\bar{H}(j\omega)$, $\bar{M}(j\omega)$, $\bar{P}(j\omega)$, $\bar{F}(j\omega)$ and $\bar{R}(j\omega)$ as their frequency response functions, using (33), (26), (28) in [22] with $\omega_d = -\omega_1$, the following expressions for maximum TVE of the positive sequence synchrophasor estimation, FE and RFE can be obtained:

$$\mathrm{TVE}_{\max} = K\max\left[|A|, P(-2j\omega_1)\right] \tag{8}$$

$$\mathrm{FE}_{\max} = KF(-j2\omega_1) \tag{9}$$

$$\mathrm{RFE}_{\max} = KR(-j2\omega_1) \tag{10}$$

being:

$$K = \frac{H\left[-j(\omega_1+\omega_0)\right]}{H\left[j(\omega_1-\omega_0)\right]}\frac{X_-}{X_+} \tag{11}$$

$$A = \tilde{M}(-j2\omega_1) - \left.\frac{dH(j\omega)}{d\omega}\right|_{\omega=\omega_1-\omega_0}\frac{2\pi\tilde{F}(-j2\omega_1)}{H\left[j(\omega_1-\omega_0)\right]} \tag{12}$$

that are obtained from (23) and (30) in [22] by considering $\omega_d = -\omega_1$. In the above equations, a complex expression without overline denotes its magnitude, while $\tilde{M}(j\omega)$ and $\tilde{F}(j\omega)$ indicate the zero-phase responses of filter M and F.

B. Reference P- and M-class algorithms

Reference P- and M-class algorithms proposed by the standard represent the second type of algorithm to be investigated. The architecture is reported in [3], but some of the parameters have been changed in the amendment [4]. The algorithms, first of all, require demodulating the phase quantities using quadrature oscillators at the rated angular frequency ω_0. Using the complex notation, recalling (3), after demodulation the three signals $\bar{x}_{a,d}$, $\bar{x}_{b,d}$ and $\bar{x}_{c,d}$ are obtained.

$$\begin{bmatrix}\bar{x}_{a,d}(t)\\ \bar{x}_{b,d}(t)\\ \bar{x}_{c,d}(t)\end{bmatrix} = \frac{1}{\sqrt{2}}\left(\begin{bmatrix}\bar{X}_a\\ \bar{X}_b\\ \bar{X}_c\end{bmatrix}e^{j(\omega_1-\omega_0)t} + \begin{bmatrix}\bar{X}_a^*\\ \bar{X}_b^*\\ \bar{X}_c^*\end{bmatrix}e^{-j(\omega_1+\omega_0)t}\right) \tag{13}$$

After that, the three synchrophasors are estimated by applying a linear phase, low pass filter H' characterized by its frequency response function $\bar{H}'(j\omega)$, and compensating for the group delay. Considering the generic phase p, it results:

$$\bar{x}_{p,e}(t) = \left[1 + \frac{\bar{H}\left[-j(\omega_1+\omega_0)\right]}{\bar{H}\left[j(\omega_1-\omega_0)\right]}e^{-j2(\omega_1 t+\varphi_p)}\right]\cdot \cdot\tilde{H}\left[j(\omega_1-\omega_0)\right]\bar{X}_p e^{j(\omega_1-\omega_0)t} \tag{14}$$

Where $\bar{H}(j\omega) = \bar{H}'(j\omega)/\sqrt{2}$, $\tilde{H}(j\omega)$ is the zero-phase response of filter H and $\bar{x}_{p,e}$ is the measured synchrophasor. The positive sequence synchrophasor is estimated using the Fortescue transformation. Recalling (4), the estimated positive sequence synchrophasor can be expressed in terms of symmetrical components.

$$\bar{x}_{+,e}(t) = \left(1 + \bar{K}e^{-j2\omega_1 t}\right)\tilde{H}\left[j(\omega_1-\omega_0)\right]\bar{X}_+ e^{j(\omega_1-\omega_0)t} \tag{15}$$

having defined:

$$\bar{K} = \frac{\bar{H}\left[-j(\omega_1+\omega_0)\right]}{\bar{H}\left[j(\omega_1-\omega_0)\right]}\frac{\bar{X}_-^*}{\bar{X}_+} \tag{16}$$

Therefore, the positive sequence synchrophasor estimation contains a disturbance proportional to the ratio between positive and negative components (unbalance level), but is completely unaffected by the zero-sequence term. Frequency and ROCOF are obtained by using the finite differences method to approximate an ideal differentiation of the phase of $\bar{x}_{+,e}$. From these computations, the maximum frequency and ROCOF errors ($\mathrm{FE}_{\max}$ and $\mathrm{RFE}_{\max}$) can be obtained:

$$\mathrm{FE}_{\max} \simeq 2Kf_1 \tag{17}$$

$$\mathrm{RFE}_{\max} \simeq 8\pi K f_1^2 \tag{18}$$

For the M-class algorithm, the TVE can be computed by comparing (15) with (5). The TVE is composed by an average value plus an oscillating term; after some computations, the peak value $\mathrm{TVE}_{\max}$ results:

$$\mathrm{TVE}_{\max} = \left|H\left[j(\omega_1-\omega_0)\right]-1\right| + KH\left[j(\omega_1-\omega_0)\right] \tag{19}$$

In this case, $\mathrm{TVE}_{\max}$ is composed by the sum of two terms: the first one is the gain error of filter H with respect to unity; the second is proportional to K, hence to the unbalance level.

As for the *P*-class reference algorithm, the FIR filter H is represented by a two-cycle triangular window resulting in significant attenuation under off-nominal frequency conditions. For this reason, the *P*-class algorithm includes an amplitude compensation of the filter output according to the estimated frequency. If the amplitude compensation exactly implements the magnitude response of H, performing a computation similar to that presented in [22] for steady-state tests, the following expression of maximum total vector error is derived:

$$\mathrm{TVE}_{\max} = K \max\left(|A|,1\right) \tag{20}$$

where:

$$A = 1 + \left.\frac{dH\left(j\omega\right)}{d\omega}\right|_{\omega=\omega_1-\omega_0} \frac{4\pi\omega_1}{H\left[j\left(\omega_1-\omega_0\right)\right]} \tag{21}$$

As a final consideration, all the derived expressions clearly show how the main effect of unbalance is the infiltration of a double frequency component due to the negative-sequence phasor into all the measurements. The effect of such disturbance is magnified by the differentiations required for frequency and ROCOF computations.

C. Taylor-Fourier Filter algorithms

Another important class of synchrophasor estimation algorithms, specifically conceived for dynamic conditions, is that considering a dynamic model given by the Taylor expansion of the phasor around the measurement reference time [23]. The discrete-time model underlying the measurement algorithm is the following one (here and in the following $\Re[\cdot]$ and $\Im[\cdot]$ indicate the real and imaginary parts, respectively):

$$\begin{aligned} x_p((m+n)T_s) &= \sqrt{2}\Re\left[\bar{x}_p((m+n)T_s)e^{j\omega_0 nT_s}\right] \\ &\simeq \sqrt{2}\Re\left[\sum_{i=0}^{k} q_{p,i}(mT_s)\frac{(nT_s)^i}{i!}e^{j\omega_0 nT_s}\right] \\ &= \frac{1}{\sqrt{2}}\left[\sum_{i=0}^{k} q_{p,i}(mT_s)\frac{(nT_s)^i}{i!}e^{j\omega_0 nT_s} + \sum_{i=0}^{k} q^*_{p,i}(mT_s)\frac{(nT_s)^i}{i!}e^{-j\omega_0 nT_s}\right] \end{aligned} \tag{22}$$

where $n = -\frac{N-1}{2},\cdots,\frac{N-1}{2}$ is the index spanning the samples of the signal x_p in the *N*-sample observation window around the measurement instant mT_s, while subscript $p \in \{a, b, c\}$ denotes the phase. The coefficient $q_{p,i}(mT_s)$ represents the generic i-derivative of the phasor $\bar{x}_p(t)$ at the instant mT_s and k is the adopted expansion order.

Rewriting (22) in matrix form, the linear model follows (the measurement time is dropped for the sake of simplicity):

$$\mathbf{x}_p = \frac{1}{\sqrt{2}}[\mathbf{\Phi}\cdot\mathbf{A}\,\mathbf{\Phi}^H\cdot\mathbf{A}]\cdot\mathbf{q}_p = \mathbf{B}\cdot\mathbf{q}_p \tag{23}$$

where $\mathbf{x}_p$ is the vector of the samples in the measurement window, $\mathbf{q}_p = [q_{p,0},\ q_{p,1},\ \cdots,\ q_{p,k},\ q^*_{p,0},\ q^*_{p,1},\ \cdots,\ q^*_{p,k}]^T$, $\mathbf{\Phi}$ is a diagonal matrix including the complex exponentials appearing in (22), and the matrix $\mathbf{A}$ is:

$$\mathbf{A} = \begin{bmatrix} 1 & +\frac{N-1}{2}T_s & \frac{1}{2}\left(\frac{N-1}{2}T_s\right)^2 & \cdots & \frac{1}{k!}\left(\frac{N-1}{2}T_s\right)^k \\ \vdots & \vdots & \vdots & & \vdots \\ 1 & 0 & 0 & & 0 \\ \vdots & \vdots & \vdots & & \vdots \\ 1 & -\frac{N-1}{2}T_s & \frac{1}{2}\left(-\frac{N-1}{2}T_s\right)^2 & \cdots & \frac{1}{k!}\left(-\frac{N-1}{2}T_s\right)^k \end{bmatrix} \tag{24}$$

The solution of (23) in the least squares sense gives the estimation of the synchrophasor along with its derivatives:

$$\hat{\mathbf{q}}_p = (\mathbf{B}^{\mathrm{H}}\mathbf{B})^{-1}\mathbf{B}\cdot\mathbf{x}_p = \mathbf{H}\cdot\mathbf{x}_p \tag{25}$$

From (25) it is clear that the estimation is linear and each row of the matrix allows performing the corresponding phasor derivative estimation. Once $\hat{\mathbf{q}}_p$ is obtained, the following expressions hold:

$$\begin{aligned} \bar{x}_{p,e} &= \hat{q}_{p,0} \\ \Delta f_{p,e} &= \frac{1}{2\pi}\frac{\Im\left[\hat{q}_{p,1}\hat{q}_{p,0}{}^*\right]}{\left|\hat{q}_{p,0}\right|^2} \\ \mathrm{ROCOF}_{p,e} &= \frac{1}{\pi}\left(\frac{\Im\left[\hat{q}_{p,2}\hat{q}_{p,0}{}^*\right]}{2\left|\hat{q}_{p,0}\right|^2} - \frac{\Re\left[\hat{q}_{p,1}\hat{q}_{p,0}{}^*\right]\Im\left[\hat{q}_{p,1}\hat{q}_{p,0}{}^*\right]}{\left|\hat{q}_{p,0}\right|^4}\right) \end{aligned} \tag{26}$$

and the desired quantities can be estimated for each phase. It can be noticed that the matrix $\mathbf{H}$ rows can be seen as containing the following filter coefficients:

$$\begin{aligned} h_0(-n) &= \mathbf{H}_{1,n} \\ h_1(-n) = \mathbf{H}_{2,n} &\quad h_2(-n) = \mathbf{H}_{3,n} \end{aligned} \tag{27}$$

used to compute $\hat{q}_{p,0}$, $\hat{q}_{p,1}$ and $\hat{q}_{p,2}$. Such filters have peculiarities due to their definition and to the property $\mathbf{H}\cdot\mathbf{B} = \mathbf{I}_{2k+2}$. Phasor estimation is performed by means of h_0 and it is easy to show that:

$$\begin{aligned} \sum_n h_0(n)e^{-j\omega_0 nT_s} &= \bar{H}_0(j\omega_0) = \sqrt{2} \\ \sum_n \left(nT_s\right)^i h_0(n)e^{-j\omega_0 nT_s} &= j^i\left.\frac{d^i\bar{H}_0}{d\omega^i}\right|_{\omega_0} = 0 \quad \text{for } 0 < i \le k \\ \sum_n \left(nT_s\right)^i h_0(n)e^{+j\omega_0 nT_s} &= j^i\left.\frac{d^i\bar{H}_0}{d\omega^i}\right|_{-\omega_0} = 0 \quad \text{for } i \le k \end{aligned} \tag{28}$$

Then the estimated phasors, relating to a single phase and the positive sequence, can be expressed similarly to (14) and (15), respectively (replacing the generic filter $\bar{H}$ with $\bar{H}_0$). For the estimated phasor of each phase it results:

$$\bar{x}_{p,e}(t)=\frac{1}{\sqrt{2}}\left(1+\bar{K}_{0,p}e^{-j2\omega_1 t}\right)\bar{H}_0(j\omega_1)\bar{X}_p e^{j(\omega_1-\omega_0)t} \quad (29)$$

where $\bar{K}_{0,p}=\dfrac{\bar{H}_0(-j\omega_1)}{\bar{H}_0(j\omega_1)}e^{-j2\varphi_n}=\bar{K}_0 e^{-j2\varphi_n}=K_0 e^{-j(2\varphi_n-\varphi_{K_0})}$.

When considering the positive sequence estimation, obtained applying the Fortescue transformation to the three estimated synchrophasors, the following expression applies (a generic time variable t is used for the sake of clarity):

$$\bar{x}_{+,e}(t)=\frac{1}{\sqrt{2}}\left(1+\bar{K}_{0,+}e^{-j2\omega_1 t}\right)\bar{H}_0(j\omega_1)\bar{X}_+ e^{j(\omega_1-\omega_0)t} \quad (30)$$

where $\bar{K}_{0,+}=\dfrac{\bar{H}_0(-j\omega_1)}{\bar{H}_0(j\omega_1)}\dfrac{\bar{X}_-}{\bar{X}_+}$. Analogously to the previous section, the maximum estimation error can be expressed, by means of TVE, as:

$$\mathrm{TVE}_{\max}=\left|\frac{\bar{H}_0(j\omega_1)}{\sqrt{2}}-1\right|+\frac{X_-}{X_+}\frac{H_0(-j\omega_1)}{\sqrt{2}} \quad (31)$$

The maximum TVE depends on the ratio between negative and positive sequence and thus involves both amplitude and phase-angle unbalance.

It is interesting to notice that, when all but the first term of the Taylor series remainder can be considered in the expansions of the filter frequency response around $\pm\omega_0$, $\bar{H}_0(j\omega_1)\simeq\sqrt{2}+\left.\dfrac{d^{k+1}\bar{H}_0}{d\omega^{k+1}}\right|_{\omega_0}\dfrac{(\omega_1-\omega_0)^{k+1}}{(k+1)!}$, while $\bar{H}_0(-j\omega_1)\simeq\left.\dfrac{d^{k+1}\bar{H}_0}{d\omega^{k+1}}\right|_{-\omega_0}\dfrac{(-\omega_1+\omega_0)^{k+1}}{(k+1)!}$, due to (28).

The above expressions of the TVE and, in the following, those relating to FE and RFE, are valid for a generic order of expansion k.

Frequency and ROCOF are estimated by the second and third expressions in (26), respectively, and such equations allow defining also the frequency and ROCOF estimation errors when $\hat{q}_{p,0}$, $\hat{q}_{p,1}$ and $\hat{q}_{p,2}$ are expressed using the corresponding filters. Focusing first on single-phase estimations, it is possible to obtain:

$$\mathrm{FE}_p(t)=\left|\Delta f_{p,e}-(f_1-f_0)\right|=\left|-(f_1-f_0)+\frac{\Im\left[\bar{H}_1(j\omega_1)\bar{H}_0^{\,*}(j\omega_1)+\bar{H}_1(j\omega_1)\bar{H}_0^{\,*}(-j\omega_1)e^{j(2\omega_1 t+2\varphi_p)}\right]}{2\pi\bar{H}_0^{\,2}(j\omega_1)\left(1+K_0\cos\left(2\omega_1 t+2\varphi_p-\varphi_{K_0}\right)\right)^2}+\frac{\Im\left[\bar{H}_1(-j\omega_1)\bar{H}_0^{\,*}(j\omega_1)e^{-j(2\omega_1 t+2\varphi_p)}+\bar{H}_1(-j\omega_1)\bar{H}_0^{\,*}(-j\omega_1)\right]}{2\pi\bar{H}_0^{\,2}(j\omega_1)\left(1+K_0\cos\left(2\omega_1 t+2\varphi_p-\varphi_{K_0}\right)\right)^2}\right| \quad (32)$$

where the denominators are $|\hat{q}_{p,0}|^2$ for $K_0<<1$.

Similarly to (28), it is possible to define the derivatives of $\bar{H}_1$ around $\pm\omega_0$. Only the first derivative $\left.\frac{d\bar{H}_1}{d\omega}\right|_{\omega_0}$ is non-zero, as follows:

$$\sum_n nT_s h_1(n)e^{-j\omega_0 nT_s}=j\left.\frac{d\bar{H}_1}{d\omega}\right|_{\omega_0}=\sqrt{2}$$

$$\sum_n\left(nT_s\right)^i h_1(n)e^{-j\omega_0 nT_s}=j^i\left.\frac{d^i\bar{H}_1}{d\omega^i}\right|_{\omega_0}=0\quad 0\le i\le k, i\ne 1 \quad (33)$$

$$\sum_n\left(nT_s\right)^i h_1(n)e^{+j\omega_0 nT_s}=j^i\left.\frac{d^i\bar{H}_1}{d\omega^i}\right|_{-\omega_0}=0\quad i\le k$$

and thus it is possible to express the filter frequency responses by means of their Taylor expansions till the order $k+1$.

After a few simplifications, the following expression can be derived:

$$\mathrm{FE}_p(t)=\left|f_1-f_0\right|\cdot\left|C_p(t)\frac{(\omega_1-\omega_0)^k}{(k+1)!}-2K_0\cos\left(2\omega_1 t+2\varphi_p-\varphi_{K_0}\right)\right| \quad (34)$$

where:

$$C_p(t)=\frac{1}{\sqrt{2}}\left(\left.\frac{d^{k+1}\Im\left[\bar{H}_1\right]}{d\omega^{k+1}}\right|_{\omega_0}+(-1)^{k+1}\left.\frac{d^{k+1}\Im\left[\bar{H}_1\right]}{d\omega^{k+1}}\right|_{-\omega_0}\cos\left(2\omega_1 t+2\varphi_p\right)-(-1)^{k+1}\left.\frac{d^{k+1}\Re\left[\bar{H}_1\right]}{d\omega^{k+1}}\right|_{-\omega_0}\sin\left(2\omega_1 t+2\varphi_p\right)\right) \quad (35)$$

Frequency estimations for each phase have been obtained; nevertheless, a set of three-phase quantities is characterized by a unique frequency value. For this reason, the frequency of the three-phase quantities is obtained as the average of the three measured frequencies and seeking an expression for the maximum frequency error, the following holds in the unbalanced system defined by (1):

$$\mathrm{FE}\le\left|f_1-f_0\right|\cdot\left[\frac{1}{\sqrt{2}}\frac{\left|\omega_1-\omega_0\right|^k}{(k+1)!}\left(\left|\left.\frac{d^{k+1}\Im\left[\bar{H}_1\right]}{d\omega^{k+1}}\right|_{\omega_0}\right|+\frac{1}{3}\left|\left.\frac{d^{k+1}\Im\left[\bar{H}_1\right]}{d\omega^{k+1}}\right|_{-\omega_0}\right|\sqrt{\left(1-\cos 2k_a\right)^2+\left(\sin 2k_a\right)^2}\right)+\frac{2}{3}K_0\left(1-\cos 2k_a\right)\right] \quad (36)$$

The error includes a first term due to off-nominal frequency and two others relating to the phase unbalance. This underlines how frequency estimation is independent from amplitude unbalance, since the frequency errors on a single phase (34) are only influenced by relative level of disturbances.

With similar passages, using (26) and the properties of the second derivative filter h_2 (zero derivatives at $\pm\omega_0$, except for the second derivative at ω_0, as required by the second order

derivation filter), it is possible to obtain the ROCOF estimation for each phase. $\mathrm{ROCOF}_{p,e}$ can be approximated as:

$$\mathrm{ROCOF}_{p,e}(t) \simeq \frac{1}{2\pi} E_p(t) \frac{(\omega_1 - \omega_0)^{k+1}}{(k+1)!} \left(1 - 2K_0 \cos\left(2\omega_1 t + 2\varphi_p - \varphi_{K_0}\right)\right) \tag{37}$$

where:

$$E_p(t) = \frac{1}{\sqrt{2}} \left(\left. \frac{d^{k+1} \Im\left[\bar{H}_2\right]}{d\omega^{k+1}} \right|_{\omega_0} + (-1)^{k+1} \left. \frac{d^{k+1} \Im\left[\bar{H}_2\right]}{d\omega^{k+1}} \right|_{-\omega_0} \cos\left(2\omega_1 t + 2\varphi_p\right) - (-1)^{k+1} \left. \frac{d^{k+1} \Re\left[\bar{H}_2\right]}{d\omega^{k+1}} \right|_{-\omega_0} \sin\left(2\omega_1 t + 2\varphi_p\right) \right) \tag{38}$$

and, by averaging with further simplifications, the following holds for an unbalanced system:

$$\mathrm{RFE}_{\max} = \max\left|\mathrm{ROCOF}_{p,e}\right| = \frac{1}{2\pi} \frac{\left|\omega_1 - \omega_0\right|^{k+1}}{(k+1)!} \frac{1}{\sqrt{2}} \left(\left| \left. \frac{d^{k+1} \Im\left[\bar{H}_2\right]}{d\omega^{k+1}} \right|_{\omega_0} \right| + \frac{1}{3} \left| \left. \frac{d^{k+1} \Re\left[\bar{H}_2\right]}{d\omega^{k+1}} \right|_{-\omega_0} \right| \sqrt{\left(1 - \cos 2k_a\right)^2 + \left(\sin 2k_a\right)^2} \right) \tag{39}$$

As for the RFE, similarly to FE, the error budget can be divided into a first term due to the deviation from nominal frequency and a second one due only to the phase unbalance, because a magnitude change on a single phase does not affect the corresponding ROCOF estimation.

D. Interpolated DFT based PMUs

Frequency-domain interpolation techniques are commonly employed for synchrophasor and frequency estimation [24]. The main advantage lies in the excellent steady-state performance, also under off-nominal frequency conditions. Let us consider the generic phase voltage or current signal $x_p(t)$, $p \in \{a, b, c\}$, as from (3), acquired with a sampling frequency $f_s = Mf_0$. A N-sample rolling window ($N = P \cdot M$, where P is the number of nominal cycles) whose order is at least equal to two, is applied to the signal. Introducing $T_w = (N-1)T_s$, the expression of the windowed signal $x_{p,w}(t,\tau)$ is obtained.

$$x_{p,w}(t,\tau) = w(\tau) x_p\left(t - T_w + \tau\right) \tag{40}$$

where τ spans from 0 to T_w in discrete steps. After some computations, the DFT of the windowed signal results:

$$\overline{X}_{p,w}\left(t, jk\omega_w\right) = \frac{1}{\sqrt{2}} \bar{X}_p e^{j\omega_1\left(t - T_w\right)} \left[\bar{W}\left(j\left(k\omega_w - \omega_1\right)\right) + \bar{W}\left(j\left(k\omega_w + \omega_1\right)\right) e^{-j2\left[\omega_1\left(t - T_w\right) - \varphi_p\right]} \right] \tag{41}$$

ω_w is the DFT angular frequency resolution and $\bar{W}(j\omega)$ the window frequency response. Let us introduce $\tilde{k}$ as the harmonic index of the greatest positive frequency spectral component and k_γ as that of the highest component adjacent to the $\tilde{k}$ th. When the usual, two-point interpolation is considered, the ratio γ between the magnitudes of these two components has to be computed. Assuming that $w(t)$ has linear-phase response (hence constant group delay τ_w), the analytic expression of γ results:

$$\gamma \simeq \gamma_0 \left[1 - K_\gamma \cos\left(2\left(\omega_1\left(t - T_w + \tau_w\right) + \varphi_p\right)\right)\right] \tag{42}$$

where:

$$\gamma_0 = \frac{W\left(j\left(k_\gamma \omega_w - \omega_1\right)\right)}{W\left(j\left(\tilde{k}\omega_w - \omega_1\right)\right)} \qquad K_\gamma = \frac{\tilde{W}\left(j\left(\tilde{k}\omega_w + \omega_1\right)\right)}{\tilde{W}\left(j\left(\tilde{k}\omega_w - \omega_1\right)\right)} - \frac{\tilde{W}\left(j\left(k_\gamma \omega_w + \omega_1\right)\right)}{\tilde{W}\left(j\left(k_\gamma \omega_w - \omega_1\right)\right)} \tag{43}$$

being $\tilde{W}(j\omega)$ the zero-phase response of the window. It should be noticed that spectral leakage results in a double-frequency alternating component in γ. The fundamental frequency $f_{p,e}$ can be estimated as:

$$f_{p,e} = \left(\tilde{k} + \Delta k_p\right) f_w \tag{44}$$

having introduced $f_w = \omega_w / 2\pi$ and Δk_p is the estimated frequency deviation of phase p in bins, obtained from a proper function $D_w(\gamma)$ depending on the weighting window. By means of a first-order expansion, the following expression of Δk_p is obtained:

$$\Delta k_p = \mathrm{sgn}\left(k_\gamma - \tilde{k}\right) D_w(\gamma) \simeq \mathrm{sgn}\left(k_\gamma - \tilde{k}\right) \left[D_w(\gamma_0) - \left. \frac{\partial D_w}{\partial \gamma} \right|_{\gamma_0} \gamma_0 K_\gamma \cos\left(2\left(\omega_1\left(t - T_w + \tau_w\right) + \varphi_p\right)\right) \right] \tag{45}$$

where sgn(·) denotes the sign function. Compensating the group delay, the estimated frequency is given by:

$$f_{p,e}\left(t - \tau_w\right) = f_1 + \mathrm{sgn}\left(\tilde{k} - k_\gamma\right) \left. \frac{\partial D_w}{\partial \gamma} \right|_{\gamma_0} \cdot \cdot \gamma_0 K_\gamma f_w \cos\left(2\left(\omega_1\left(t - T_w + \tau_w\right) + \varphi_p\right)\right) \tag{46}$$

Thus, phase p maximum frequency error results:

$$\mathrm{FE}_{p,\max} = \left| \left. \frac{\partial D_w}{\partial \gamma} \right|_{\gamma_0} K_\gamma \right| \gamma_0 f_w \tag{47}$$

The ROCOF can be obtained through differentiation, for example by means of the finite differences method. Its analytic expression as well as that of the RFE comes straightforwardly.

The synchrophasor magnitude $x_{p,e}$ is computed by compensating the group delay and the scalloping loss from the $\tilde{k}$ -th component of the DFT:

$$x_{p,e}\left(t-\tau_w\right)=\sqrt{2}\frac{X_{p,w}\left(t,j\tilde{k}\omega_w\right)}{W\left(j\Delta k_p\omega_w\right)} \tag{48}$$

After some computations and first-order approximations:

$$\begin{aligned}x_{p,e}\left(t-\tau_w\right)\simeq X_{1,n}\Bigg\{1+\frac{1}{\tilde{W}\left(j\left(\tilde{k}\omega_w-\omega_1\right)\right)}\Bigg[\tilde{W}\left(j\left(\tilde{k}\omega_w+\omega_1\right)\right)+\\ +\operatorname{sgn}\left(\tilde{k}-k_\gamma\right)\frac{\partial D_w}{\partial\gamma}\bigg|_{\gamma_0}\frac{\partial W}{\partial\omega}\bigg|_{\tilde{k}\omega_w-\omega_1}\gamma_0\omega_w K_\gamma\Bigg]\cos\left(2\left(\omega_1\left(t-T_w+\tau_w\right)+\varphi_p\right)\right)\Bigg\}\end{aligned} \tag{49}$$

Also the synchrophasor phase angle $\theta_{p,e}$ is derived from the $\tilde{k}$ th component of the DFT, having properly compensated the delays due to DFT and windowing:

$$\begin{aligned}\theta_{p,e}\left(t-\tau_w\right)=\varphi_p+\left(\omega_1-\omega_0\right)t+\left(\omega_0+\tilde{k}\omega_w\right)\tau_w-\omega_1T_w+2\pi f_{p,e}\left(T_w-2\tau_w\right)+\\ +\angle\left[\bar{W}\left(j\left(\tilde{k}\omega_w-\omega_1\right)\right)+\bar{W}\left(j\left(\tilde{k}\omega_w+\omega_1\right)\right)e^{-j2\left(\omega_1\left(t-T_w\right)+\varphi_p\right)}\right]\end{aligned} \tag{50}$$

The term containing the estimated frequency appears when the group delay is not exactly half of the window length, for example when a periodic window is employed. In this case, T_w-$2\tau_w$=T_s, therefore this contribution can be neglected for high sampling rates. After some computations:

$$\begin{aligned}\theta_{p,e}\left(t-\tau_w\right)\simeq\varphi_p+\left(\omega_1-\omega_0\right)\left(t-\tau_w\right)+\\ -\frac{\tilde{W}\left(j\left(\tilde{k}\omega_w+\omega_1\right)\right)}{\tilde{W}\left(j\left(\tilde{k}\omega_w-\omega_1\right)\right)}\sin\left(2\left(\omega_1\left(t-T_w+\tau_w\right)+\varphi_p\right)\right)+\\ +\operatorname{sgn}\left(\tilde{k}-k_\gamma\right)\frac{\partial D_w}{\partial\gamma}\bigg|_{\gamma_0}\gamma_0K_\gamma\omega_w\left(T_w-2\tau_w\right)\cos\left(2\left(\omega_1\left(t-T_w+\tau_w\right)+\varphi_p\right)\right)\end{aligned} \tag{51}$$

Having obtained the phase p synchrophasor in terms of magnitude and phase angle, the TVE can be obtained. Its expression is quite complicated and not reported for the sake of brevity. However, a simple, approximated expression of the maximum TVE can be derived:

$$\mathrm{TVE}_{p,\max}\simeq\frac{W\left(j\left(\tilde{k}\omega_w+\omega_1\right)\right)}{W\left(j\left(\tilde{k}\omega_w-\omega_1\right)\right)} \tag{52}$$

Analytic expressions for the frequency and ROCOF estimations for each phase have been obtained; frequency and ROCOF of the three-phase quantities are computed by averaging the three single-phase measurements.

Let us start with the frequency estimation. Using (46), substituting the phasor magnitudes and angles reported in (1) while taking the average of the three estimations, the expression of the frequency is obtained. The peak frequency error results:

$$\mathrm{FE}_{\max}=\frac{\sqrt{2}}{3}\left|\frac{\partial D_w}{\partial\gamma}\bigg|_{\gamma_0}K_\gamma\right|\gamma_0f_w\sqrt{1-\cos\left(2k_a\right)} \tag{53}$$

As expected (like in Section II.C), the frequency estimation obtained by averaging three single-phase measurements is not affected by magnitude unbalance. It is worth noticing that by using the approximated expressions, and in absence of phase-angle unbalance, the double-frequency components due to leakage in the single-phase frequency estimations cancel out thanks to the average. Being the ROCOF obtained by differentiation, the expression of $\mathrm{RFE}_{\max}$ is obtained immediately.

Finally, an analytic expression of the positive sequence synchrophasor can be obtained using (1), (49), (51) and applying the Fortescue transformation. The TVE can be obtained, but the equation is rather complex and a simple yet accurate expression of the peak value is available for the magnitude unbalance only:

$$\mathrm{TVE}_{\max}\simeq\frac{|k_x|}{3+k_x}\frac{W\left(j\left(\tilde{k}\omega_w+\omega_1\right)\right)}{W\left(j\left(\tilde{k}\omega_w-\omega_1\right)\right)} \tag{54}$$

III. Tests and Results

The measurement performances of the different techniques in the presence of unbalance have been compared by means of numerical simulations, which also permit to validate the analytic expressions of the maximum errors derived in Section II. The conditions resemble those suggested by [12], thus the test signals are obtained from three perfectly balanced sinusoids, having frequency f_1, by changing the magnitude or angle of one of them. In particular:

- Magnitude variation k_x: ±10% and ±20%, corresponding to about 3% and 6% unbalance levels.
- Phase-angle variation k_a: ±20°, ±40° and ±60°, namely 11%, 24% and 38% unbalance levels.
- Fundamental frequency f_1: f_0 and f_0-1 Hz (50 Hz and 49 Hz for 50 Hz systems).

For each kind of algorithm, two implementations have been tested: one designed to provide low latency and fast response times, the other tailored to ensure high steady-state accuracy. When available, the P- and M-class versions of the algorithms (for the maximum reporting rate stated in [3], that is 50 frames/s for a nominal system frequency of 50 Hz) have been used, otherwise two different window lengths have been adopted, inspired by those of the filters suggested in [3] for the two classes.

As for SV algorithms, the following configurations implemented with a $f_s=16\cdot f_0$ sampling frequency (same as in [22]) have been tested:

- P-SV: 2 Hz passband frequency and 50 Hz stopband frequency for *H, M, P, F* and *R* filters. Passband ripple $2\cdot10^{-3}$ for *H*, 10^{-2} for *M* and *P*. Stopband ripple $3\cdot10^{-2}$ for *H, M* and *P*. Filter order 36 and stopband weights 100 and 1000, respectively for *F* and *R*.
- M-SV: 5 Hz passband frequency and 25 Hz stopband frequency for *H, M, P, F* and *R*.

Passband ripple $2\cdot10^{-3}$ for *H*, 10^{-2} for *M* and *P*. Stopband ripple $3\cdot10^{-2}$ for *H,* 10^{-2} for *M* and *P*. Filter order 128 and stopband weights 100 and 1000, respectively for *F* and *R*.

The P- and M-class reference algorithms proposed by the standard have been implemented and tested with a sampling rate $f_s = 16 \cdot f_0$. In the following, they are indicated as P-C37.118 and M-C37.118, respectively.

Two- and six-cycle Taylor-Fourier algorithms have been considered, and denoted as 2-TF and 6-TF in the following. Both of them have been implemented with the usual $f_s = 16 \cdot f_0$ sampling frequency using a second order expansion, the minimum that allows performing both frequency and ROCOF estimations without turning to discrete-time derivatives.

The considered IpDFT implementations are based on periodic Hann windows that allow considerably better performance with respect to the symmetric versions. As explained in Section II.D, with this choice the phase delay compensation depends on the estimated frequency, resulting in an additional error contribution evident in (50) and (51). Since this term is inversely proportional to the sampling rate, $f_s = 200 \cdot f_0$ has been employed so that its impact results to be very small. Two-cycle and six-cycle implementations have been studied, and are denoted as 2-IpDFT and 6-IpDFT.

For all the tests and algorithms, the maximum TVE, FE and RFE have been computed using 1-second test signals and sample-by-sample estimations. Since all the unbalance tests are steady-state tests, using a time resolution equal to the sampling interval allows better determining the maxima without changing the initial phase angle.

First of all, the impact of unbalance on low-latency PMU algorithms is analyzed. Table I reports the maximum percent TVE for the positive sequence phasor estimation, the maximum FE and RFE for the above test cases as well as in symmetrical test conditions with 49 Hz frequency. Error values at 50 Hz without unbalance are not reported since they are negligible for all the algorithms. Results are compared with the values (between round brackets) derived by means of the analytic expressions proposed in Section II. For the amplitude unbalance tests, only the results for negative variations are reported: being characterized by higher unbalance level, for all the algorithms they have a greater impact on the estimations. When looking at (8)-(10) and (17), (18), (20), it can be noticed that maximum TVE, FE and RFE of the reference algorithms and of the SV-based techniques are proportional to X_- / X_+, namely the unbalance level. From (2) it immediately appears that this ratio is higher for the negative amplitude changes. Furthermore, higher errors in the phase unbalance tests are expected, being them characterized by higher unbalance levels.

TABLE I. IMPACT OF MAGNITUDE AND PHASE UNBALANCE ON LOW-LATENCY PMU ALGORITHMS

Method	Freq [Hz]	k_x [%]	k_a [°]	Max Errors		
				TVE [%]	FE [mHz]	RFE [Hz/s]
P-C37.118	49	0	0	7.3e-4 (0.0000)	0.000 (0.000)	0.000 (0.000)
		-10	0	0.0012 (0.0005)	0.328 (0.363)	0.213 (0.223)
		-20	0	0.0017 (0.0009)	0.679 (0.751)	0.440 (0.463)
		0	+20	0.0023 (0.0016)	1.12 (1.23)	0.723 (0.760)
		0	+40	0.0039 (0.0032)	2.29 (2.53)	1.48 (1.56)
		0	+60	0.0057 (0.0050)	3.59 (3.98)	2.33 (2.45)
P-SV	50	-10	0	2.5e-4 (2.4e-4)	0.012 (0.012)	0.0083 (0.0083)
		-20	0	5.1e-4 (5.1e-4)	0.025 (0.025)	0.017 (0.017)
		0	+20	8.5e-4 (8.3e-4)	0.040 (0.042)	0.027 (0.028)
		0	+40	0.0018 (0.0017)	0.084 (0.086)	0.057 (0.058)
		0	+60	0.0029 (0.0027)	0.134 (0.134)	0.091 (0.091)
	49	0	0	0.0000 (0.0000)	0.000 (0.000)	0.000 (0.000)
		-10	0	4.9e-4 (4.9e-4)	0.0039 (0.0039)	0.0038 (0.0039)
		-20	0	0.0010 (0.0010)	0.0080 (0.0080)	0.0082 (0.0082)
		0	+20	0.0017 (0.0017)	0.013 (0.013)	0.013 (0.013)
		0	+40	0.0036 (0.0034)	0.027 (0.027)	0.028 (0.027)
		0	+60	0.0058 (0.0054)	0.044 (0.042)	0.043 (0.043)
2-TF	49	0	0	0.37e-4 (0.37e-4)	1.59 (1.59)	0.000 (0.000)
		-10	0	0.58e-4 (0.58e-4)	1.59 (1.59)	0.000 (0.000)
		-20	0	0.80e-4 (0.80e-4)	1.59 (1.59)	0.000 (0.000)
		0	+20	1.1e-4 (1.1e-4)	1.64 (1.65)	0.0082 (0.0073)
		0	+40	1.8e-4 (1.8e-4)	1.69 (1.69)	0.015 (0.014)
		0	+60	2.6e-4 (2.6e-4)	1.72 (1.72)	0.021 (0.019)
2-IpDFT	49	0	0	2.3e-4 (0.0000)	0.021 (0.000)	7.8e-5 (0.000)
		-10	0	0.0024 (0.0024)	0.021 (0.000)	2.4e-4 (0.000)
		-20	0	0.0049 (0.0049)	0.021 (0.000)	2.4e-4 (0.000)
		0	+20	0.0097 (0.0096)	15.3 (15.4)	9.48 (9.45)
		0	+40	0.0193 (0.0191)	28.8 (28.9)	17.8 (17.8)
		0	+60	0.0289 (0.0287)	38.9 (38.9)	24.0 (23.9)

FE and ROCOF estimations obtained by means of Taylor-Fourier filtering are not sensitive to magnitude unbalance, while from (31) it appears that the maximum TVE increases with the ratio X_- / X_+. As for the IpDFT techniques, from (54) it is clear that k_x<0 produces higher TVE for a given amplitude change, while frequency and ROCOF estimations are expected to be unaffected by magnitude unbalance. The

results of the P-C37.118, 2-TF and 2-IpDFT algorithms when the test signals have the nominal system frequency are not reported because they are almost zero, due to the zeros of the adopted filters.

In general, all the algorithms show very good performance in terms of TVE even when the input frequency is equal to 49 Hz: as shown in Fig. 1, the values are lower than 0.03%, thus negligible from a practical point of view.

On the contrary, unbalance has a significant impact, in particular under off-nominal frequency conditions, on frequency (Fig. 2) and ROCOF estimations. The reference and the SV-based algorithm use a similar approach for frequency and ROCOF estimations, which are obtained by differentiating the phase angle of the positive sequence synchrophasor. Unbalance results in a double-frequency ripple in its phase angle whose amplitude is increased by the differentiating filter employed to compute frequency and ROCOF. As for the P-class algorithm, unbalance leads to unacceptable errors, in particular for the estimated ROCOF, since the filters do not provide enough attenuation of this double-frequency component that acts as a third-harmonic disturbance. On the contrary, the P-SV is designed with approximated first and second order differentiators that allow a good rejection of the third harmonic, even under off-nominal frequency conditions.

The two-cycle TF filter shows fairly high frequency errors that weakly depend on the unbalance level, both in magnitude and phase. When looking at (36), this means that the error contribution due to a frequency different from the rated one is considerably higher than that due to unbalance. Conversely, ROCOF estimation is not affected by magnitude unbalance, and errors are low even in case of phase-angle unbalance.

As for the two-cycle IpDFT, results show a weak sensitivity to magnitude unbalance, but phase unbalance produces very high FE and RFE.

The analytic formulas allow, generally, a good prediction of the errors. Slight discrepancies can be found for the expected TVE of the P-C37.118 algorithm because the theoretical expressions assume ideal compensation of the scalloping loss. Further refinement can be performed by considering the empirical one proposed by the standard. The results in terms of FE and RFE for the standard algorithm are instead slightly affected by the shape of the differentiator filters: ideal differentiation was supposed to simplify the analytic expressions, but the finite difference frequency response can be also easily kept into account. As for the IpDFT, analytic expressions predict perfectly zero frequency error without phase-angle unbalance. In fact, having linearized (46), the errors in the single-phase frequency estimations due to spectral leakage perfectly cancel out when the average is computed in order to obtain the three-phase frequency. Actually, higher-order effects may produce bias and alternating components having frequency multiple of $6f_1$ that cannot be erased by averaging, thus affecting also the ROCOF estimation as evident from the results. In any case, it can be noticed that, as expected, FE and RFE do not depend on magnitude unbalance.

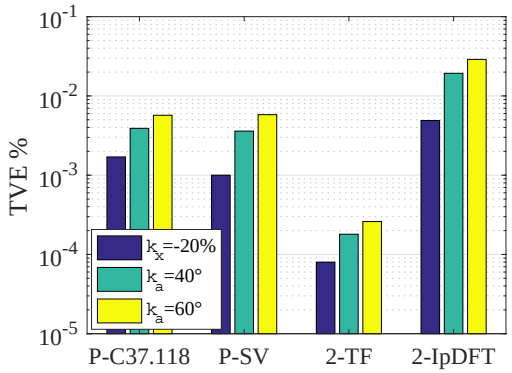

Figure 1. TVE % for low-latency algorithms: $f_0 = 49$ Hz, different unbalance conditions.

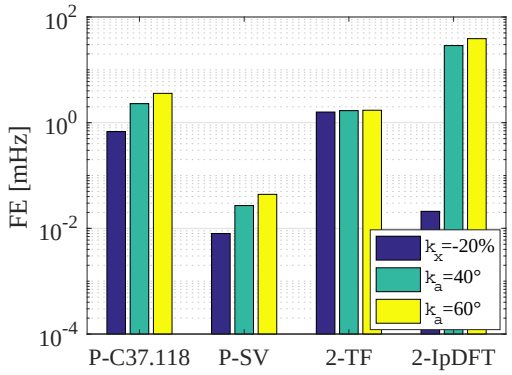

Figure 2. FE for low-latency algorithms: $f_0 = 49$ Hz, different unbalance conditions.

Table II shows the results for the same test cases, when high-accuracy algorithms are considered. Positive-sequence synchrophasor estimation is accurate for all the algorithms even under off-nominal frequency conditions, as highlighted by Fig. 3. The M-C37.118 algorithm achieves the largest errors, and this applies also to frequency and ROCOF measurements, even at nominal frequency. This is due to the characteristics of the M-class filter that is designed with the constraint of a minimum attenuation of -57.8 dB in the stopband, irrespective of the frequency of the zeros of the frequency response. The frequency errors obtained by using the six-cycle TF filter are quite large and almost independent from the unbalance. Like before, this means that these errors are almost only due to the test frequency which is different from the rated one. On the contrary, ROCOF errors are small, and practically null in case of magnitude unbalance. These results highlight, as described by the equations in Section II.C, how the errors strongly depend on the derivation filters order and shape, in particular when negative frequencies are considered. Besides, the effect of averaging among the three phases plays a crucial role in canceling balanced errors. The six-cycle IpDFT shows excellent frequency estimation, but a non-negligible ROCOF error in case of phase-angle unbalance.

Fig. 4 compares the frequency errors achieved by the considered high-accuracy algorithms in presence of unbalance, when the frequency is equal to 49 Hz. The SV-based method, thanks to the approximated differentiator, results in the lowest frequency and ROCOF errors.

TABLE II. IMPACT OF MAGNITUDE AND PHASE UNBALANCE ON HIGH-ACCURACY PMU ALGORITHMS

Method	Freq [Hz]	k_x [%]	k_a [°]	Max Errors		
				TVE [%]	FE [mHz]	RFE [Hz/s]
M-C37.118	50	-10	0	0.0011 (0.0011)	1.03 (1.14)	0.683 (0.719)
		-20	0	0.0024 (0.0024)	2.13 (2.13)	1.41 (1.49)
		0	+20	0.0039 (0.0039)	3.36 (3.89)	2.23 (2.45)
		0	+40	0.0080 (0.0080)	7.04 (7.99)	4.67 (5.02)
		0	+60	0.0125 (0.0125)	11.3 (12.5)	7.46 (7.88)
	49	0	0	0.0023 (0.0023)	0.000 (0.000)	0.000 (0.000)
		-10	0	0.0042 (0.0042)	1.73 (1.92)	1.12 (1.18)
		-20	0	0.0063 (0.0063)	3.59 (3.97)	2.33 (2.45)
		0	+20	0.0089 (0.0089)	5.90 (6.53)	3.82 (4.02)
		0	+40	0.0159 (0.0159)	12.1 (13.4)	7.85 (8.25)
		0	+60	0.0237 (0.0237)	19.0 (21.0)	12.3 (12.9)
M-SV	50	-10	0	4.5e-4 (4.5e-4)	0.0026 (0.0026)	0.26e-4 (0.26e-4)
		-20	0	9.4e-4 (9.2e-4)	0.0053 (0.0053)	0.54e-4 (0.54e-4)
		0	+20	0.0016 (0.0015)	0.0083 (0.0087)	0.85e-4 (0.89e-4)
		0	+40	0.0034 (0.0031)	0.018 (0.018)	1.8e-4 (1.8e-4)
		0	+60	0.0056 (0.0049)	0.028 (0.028)	2.9e-4 (2.9e-4)
	49	0	0	0.0000 (0.0000)	0.000 (0.000)	0.000 (0.000)
		-10	0	2.1e-4 (2.1e-4)	0.0035 (0.0035)	0.36e-4 (0.36e-4)
		-20	0	4.4e-4 (4.4e-4)	0.0073 (0.0073)	0.75e-4 (0.75e-4)
		0	+20	7.3e-4 (7.2e-4)	0.012 (0.012)	1.2e-4 (1.2e-4)
		0	+40	0.0015 (0.0015)	0.025 (0.025)	2.5e-4 (2.5e-4)
		0	+60	0.0025 (0.0023)	0.039 (0.039)	4.0e-4 (4.0e-4)
6-TF	49	0	0	0.0069 (0.0069)	14.3 (14.4)	0.000 (0.000)
		-10	0	0.0073 (0.0073)	14.3 (14.4)	0.000 (0.000)
		-20	0	0.0077 (0.0077)	14.3 (14.4)	0.000 (0.000)
		0	+20	0.0083 (0.0083)	14.4 (14.5)	0.014 (0.012)
		0	+40	0.0098 (0.0098)	14.5 (14.6)	0.026 (0.023)
		0	+60	0.0114 (0.0114)	14.5 (14.8)	0.035 (0.030)
6-IpDFT	49	0	0	0.0000 (0.0000)	1.9e-5 (0.000)	0.000 (0.000)
		-10	0	2.5e-4 (2.5e-4)	1.9e-5 (0.000)	0.000 (0.000)
		-20	0	5.1e-4 (5.1e-4)	1.9e-5 (0.000)	0.000 (0.000)
		0	+20	0.0011 (0.0011)	0.302 (0.302)	0.186 (0.186)
		0	+40	0.0022 (0.0022)	0.568 (0.568)	0.349 (0.350)
		0	+60	0.0032 (0.0032)	0.765 (0.765)	0.471 (0.471)

Except for the slight differences due to the discrete differentiators, the theoretical expressions presented in Section II.D ensure a good prediction of the errors in the presence of unbalance and can help in the design of suitable filters for the PMUs. Also in this case, it can be noticed that the IpDFT algorithm does not result in exactly zero frequency and ROCOF errors: the reason has been previously explained.

From the analytic expressions, it is possible to see how the level of unbalance can clearly affect the frequency and ROCOF measurements in practical conditions. For instance, at 48 Hz (the limit of the P-class frequency range) a 1.6% negative sequence component is sufficient, when P-C37.118 algorithm is used, to violate the limit (0.4 Hz/s) prescribed by [3] for the RFE of P-class in steady-state conditions, without considering any other disturbance such as input noise or residual harmonic distortion. For the M-class, all the limits for RFE in case of harmonic or interharmonic disturbances have been suspended by the amendment [4], but when the reference algorithm is concerned, a 0.5% negative sequence component leads, even at nominal frequency and without harmonics, to a maximum RFE higher than the 0.1 Hz/s limit for steady-state conditions.

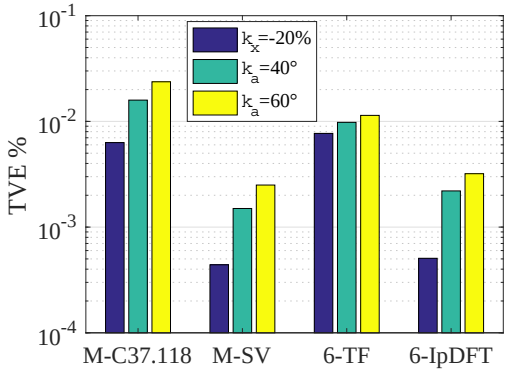

Figure 3 - TVE % for high-accuracy algorithms: $f_0 = 49$ Hz, different unbalance conditions.

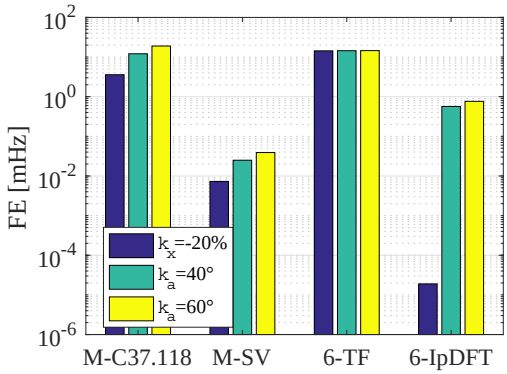

Figure 4 - FE for high-accuracy algorithms: $f_0 = 49$ Hz, different unbalance conditions.

IV. CONCLUSION

The paper presents analytic expressions that allow predicting the impact of unbalanced three-phase inputs on the

performance of different PMU algorithms, designed to measure the positive sequence synchrophasor, frequency and ROCOF. Four techniques that have recently risen in the context of synchrophasor measurements are investigated. Their performance in terms of TVE, FE and RFE are assessed by means of simulations using the test signals suggested by IEEE C37.242-2013 guide.

The theoretical analysis indicates that the influence of unbalance is radically different for each algorithm, depending on its capability to reject the equivalent harmonic disturbance. All the methods relying on a filtering approach for synchrophasor estimation (C37.118, SV and TF algorithms) are directly affected by the harmonic pollution induced by the negative sequence component due to unbalance. IpDFT instead starts from the estimation of frequency and thus the influence of amplitude and phase-angle unbalance on phasor estimation is more cumbersome and becomes more evident in case of phase-angle impairments. It is not possible to define a general rule, but it is obvious that the choice of filters and windows is of crucial importance in this context.

Frequency and ROCOF measurements are particularly sensitive to unbalance (especially to phase-angle unbalance), but to a different extent, depending on filter characteristics or on the procedure to evaluate compensation terms. The presented analytic expressions allow predicting different error contributions, thus helping the design of modern PMUs that are expected to be employed also in distribution systems, where voltages and currents unbalance levels are considerably higher.

REFERENCES

[1] Stewart, E. M. and von Meier, A, "Phasor Measurements for Distribution System Applications,". Smart Grid Handbook. 1–10.

[2] G. Frigo, D. Colangelo, A. Derviškadić, M. Pignati, C. Narduzzi and M. Paolone, "Definition of Accurate Reference Synchrophasors for Static and Dynamic Characterization of PMUs," in IEEE Transactions on Instrumentation and Measurement, vol. 66, no. 9, pp. 2233-2246, Sept. 2017.

[3] *IEEE Standard for Synchrophasor Measurements for Power Systems*, IEEE Std C37.118.1-2011.

[4] *IEEE Standard for Synchrophasor Measurements for Power Systems* -- Amendment 1: Modification of Selected Performance Requirements, IEEE Std C37.118.1a-2014 (Amendment to IEEE Std C37.118.1-2011).

[5] C. Muscas and P. A. Pegoraro, "Algorithms for synchrophasors, frequency, and rocof," in Phasor Measurement Units and Wide Area Monitoring Systems, 1st ed., A. Monti, C. Muscas, and F. Ponci, Eds. Elsevier, Academic Press, 2016, ch. 3, pp. 21–51.

[6] P. Castello, M. Lixia, C. Muscas and P. A. Pegoraro, "Impact of the Model on the Accuracy of Synchrophasor Measurement," *IEEE Trans. Instrum. Meas.*, vol. 61, no. 8, pp. 2179-2188, Aug. 2012.

[7] G. Barchi, D. Macii and D. Petri, "Synchrophasor Estimators Accuracy: A Comparative Analysis," *IEEE Trans. Instrum. Meas.*, vol. 62, no. 5, pp. 963-973, May 2013.

[8] P. Castello, C. Muscas, P. A. Pegoraro, S. Sulis and S. Toscani, "Experimental characterization of dynamic methods for synchrophasor measurements," *Proc. IEEE Int. Workshop on Appl. Meas. for Pow. Sys. (AMPS)*, Aachen, 2014, pp. 1-6.

[9] D. Gallo, C. Landi, M. Luiso, P. Tosato, D. Macii, D. Brunelli, "A Testbed for the Experimental Characterization of Estimation Algorithms for Phasor Measurement Units," *Proc. IEEE Int. Workshop on Appl. Meas. for Pow. Sys. (AMPS)*, Liverpool, 2017.

[10] A. J. Roscoe, "Exploring the Relative Performance of Frequency-Tracking and Fixed-Filter Phasor Measurement Unit Algorithms Under C37.118 Test Procedures, the Effects of Interharmonics, and Initial Attempts at Merging P-Class Response With M-Class Filtering," in IEEE Transactions on Instrumentation and Measurement, vol. 62, no. 8, pp. 2140-2153, Aug. 2013.

[11] D. Macii, D. Fontanelli, G. Barchi and D. Petri, "Impact of Acquisition Wideband Noise on Synchrophasor Measurements: A Design Perspective," in IEEE Transactions on Instrumentation and Measurement, vol. 65, no. 10, pp. 2244-2253, Oct. 2016.

[12] "IEEE Guide for Synchronization, Calibration, Testing, and Installation of Phasor Measurement Units (PMUs) for Power System Protection and Control," IEEE Std C37.242-2013, pp. 1–107, Mar. 2013.

[13] Terna SpA - Qualità del Servizio di Trasmissione - Livelli attesi della qualità della Tensione per l'anno 2017." [Online]. Available: https://www.terna.it/it-it/sistemaelettrico/qualit%C3%A0delservizioditrasmissione.aspx.

[14] R. Yan and T. K. Saha, "Investigation of Voltage Imbalance Due to Distribution Network Unbalanced Line Configurations and Load Levels," *IEEE Trans. Power Syst.*, vol. 28, pp. 1829-1838, May 2013.

[15] EN 50160 – "Voltage characteristics of electricity supplied by public distribution networks", 2010.

[16] J. Depablos, V. Centeno, A. G. Phadke and M. Ingram, "Comparative testing of synchronized phasor measurement units,"in *Proc. Power Engineering Society General Meeting,* June 2004, vol. 1, pp. 948-954.

[17] M. Karimi-Ghartemani, M. Mojiri, A. Bakhshai and P. Jain, "A phasor measurement algorithm based on phase-locked loop," in *Proc. Transmission and Distribution Conf. and Expo.,* May 2012, pp. 1-6.

[18] T. Routtenberg, Y. Xie, R. M. Willett and L. Tong, "PMU-Based Detection of Imbalance in Three-Phase Power Systems," *IEEE Trans. on Power Syst.*, vol. 30, pp. 1966-1976, July 2015.

[19] F. Messina, P. Marchi, L. Rey Vega, C. G. Galarza and H. Laiz, "A Novel Modular Positive-Sequence Synchrophasor Estimation Algorithm for PMUs," *IEEE Trans. Instrum. Meas.*, vol. 66, no. 6, pp. 1164-1175, June 2017.

[20] P. Castello, R. Ferrero, P. A. Pegoraro, S. Toscani, "Phasor Measurement Units Performance in Three-Phase Unbalanced Systems," in *Proc. Int. Instrumentation and Measurement Technology Conf.*, May 2017.

[21] S. Toscani and C. Muscas, "A space vector based approach for synchrophasor measurement," in *Proc. Int. Instrumentation and Measurement Technology Conf.*, May 2014, pp. 257–261.

[22] S. Toscani, C. Muscas and P. A. Pegoraro, "Design and performance prediction of space vector based PMU algorithms," *IEEE Trans. on Instrum. Meas.*, vol. 66, pp. 394-404, Mar. 2017.

[23] J. A. de la O Serna, "Dynamic Phasor Estimates for Power System Oscillations," in IEEE Transactions on Instrumentation and Measurement, vol. 56, no. 5, pp. 1648-1657, Oct. 2007.

[24] D. Belega and D. Petri, "Accuracy Analysis of the Multicycle Synchrophasor Estimator Provided by the Interpolated DFT Algorithm," *IEEE Trans. Instrum. Meas.*, vol. 62, no. 5, pp. 942-953, May 2013.